Nonlinear potentiodynamic battery charging protocols for fun, education, and application

Helge Sören Stein[1,*]

[1]: Technical University Munich, TUM School of Natural Sciences, Department of Chemistry, Munich Data Science Institute

*correspondence should be addressed to: helge.stein@tum.de

Abstract

Most secondary batteries in academia are (dis)charged by applying a constant current (CC) followed by a constant voltage (CV) i.e. a CCCV procedure. The usual concept is then to condense data for interpretation into representations such as differential capacity, or dQ/dV, graphs. This is done to extract information related to phenomena such as the growth of the solid electrolyte interphase (SEI) or, more broadly, degradation. Typically, these measurements take several months because measurements for differential capacity analysis need to be performed at relatively low C-rates. An alternate charging schedule to CCCV is pulsed charging, where CC sections are interrupted by an open-circuit measurement on the second time scale. These and similar partially constant current strategies primarily target diffusive effects during charging and broadly fall into a linear charging category, where the time derivative for the actuated property is mostly zero. Herein, I explore nonlinear charging i.e., the process of actively applying a potential with a nontrivial time derivate and a resulting non-trivial current time derivative to engineer (dis)charge cycles with enhanced information density. This method of non-linear charging is then used to charge a cell such that some potential ranges in the differential capacity diagram are omitted. This study is purely a simulative endeavor and not backed by experimentation, owing mainly to the lack of facile implementation of arbitrary function inputs for battery cyclers and might point to limitations of the underlying theory. If found to be confirmed through an experiment, this technique would, however motivate a new roadmap to better understand secondary battery degradation inspired by electrocatalyst degradation.

Introduction

Secondary batteries are a fascinating research topic, as findings on the lab scale have a realistic potential to impact the electrification of everything[1]. Therefore, great efforts are being undertaken across different domains, i.e., everything from ab initio calculations[2,3] on the atomic level[4] to manufacturing improvements through defect detection[5]. A European effort to bring together this multimodal and multidisciplinary research is the Battery2030+[1] initiative, namely the battery interphase genome – materials acceleration platform[3]. The idea is to discover and

optimize batteries by jointly bringing together theory and experiment in workflows[6] that allow to seamless translation between the scales[7] through the utilization of machine learning[2], artificial intelligence and lab automation[8] into a true materials acceleration platform[6]. The established workflow to optimize[9–11] systems such as batteries is, however, to look at isolated parts of the complex system i.e. to optimize electrolyte conductivity[8], reduce defect concentration[5] on coated electrodes or to test whether or not an additive prolongs the cycle life of a battery[12]. Sometimes, these methods rely on machine learning methods[13–16] as the underlying physics are either not understood or very complex to model, or experiments are too costly. If there are, however, in principle, physical laws that connect complex data like UV-Vis absorption spectra[17] and RGB images, then machine learning models work great as errors and uncertainties are low and manageable. More importantly are also benchmarks that enable scientists to both gamify research and break models in creative ways[18]. In the battery research field one of the prime examples is the optimization[19] of fast charging schedules[20] that try to mitigate cell degradation[21] despite high-charging currents. There is of course, an immediate use of these fast-charging methods e.g. for electrified (cargo) bicycles for delivery services. Other examples for machine learning in the battery domain include the prediction of remaining cell life with uncertainty quantification, as demonstrated by Rieger et al.[22] or optimization of electrolyte conductivity[8].

As discussed in Rohr et al.[19] and Stein & Gregoire[23] there are essentially four research modes for opmizitation and discovery with active learning in materials science and engineering i.e.

I. Finding *a* good parameter set/material
II. Finding *all* good parameter sets/materials
III. *Predict* parameters/materials well
IV. *Understand* the underlying physics/chemistry

The optimization studies cited above broadly fall into research modes I-III and only hint at “the ultimate” research mode IV. One notable example for directly performing research mode IV is shown in Flores et al.[24] that try to derive the laws governing electrolyte conductivity in complex solvation structures[25] from data. In this manuscript, we seek to explore if we can engineer electrochemical experiments for generating maximally information-dense data or if there is the possibility to engineer a charging procedure that is more amendable to both machine learning studies and human interpretation than CCCV.

The motivation behind this is that my research group is in fact capable of producing several orders of magnitude more batteries[26] in our laboratory[7] than we can test, necessitating either truly chemistry-neutral machine learning models[1] for early lifetime prediction[21] to shorten tests, or engineer new electrochemical processes that tell us our desired information faster. Herein I explore the latter.

One of the most informative, or insight-dense, graphs one can obtain from "off-the-shelf" CCCV-cycling of a cell is the differential capacity[27,28] or dQ/dV plot. Linear and non-linear charge procedures can sometimes yield hard-to-interpret or even hard to generate dQ/dV plots, which, given the herein demonstrated methods, might become easier to interpret and extract from data.

The phenomenological investigations herein are motivated by an educational background in electrochemistry for electrocatalysts, that corrosion is, on a first-order approximation, defined by the time spent at a potential. Yet, studies that aim to investigate or mitigate corrosion (or degradation) in batteries[20] actuate on current and not potential to mitigate corrosion. This manuscript concludes with what I believe to be a prototype building block for a Pourbaix diagram for batteries.

Methods

Simulation

All data in this manuscript stems from simulations using the pybamm[29] python package with a non-thermally lumped Doyle-Fuller-Newman model on the parameter set provided by O'Kane et al.[30] The simulated cell is a "LG M50T cylindrical cell" with graphite ande that has 10% SiO_x by mass. The cathode consists of NMC 8:1:1. All simulations were carried out on a MacBook Pro with a M2 Max Processor.

Data analysis

All data analysis is performed using python with standard off-the-shelf numpy and scipy. Differential capacity plots are obtained by integrating the current over time using the scipy function cumtrapz and the dQ/dV data is obtained from numpy gradient with a second-order polynomial. Wherever necessary, data has been interpolated using the interp1d function from scipy.

Data and Code availability

The jupyter lab notebook to simulate all cells and generate all figures is going to be available upon publication at www.github.com/helgestein/nonlinearcharging. Comments and improvements through git requests are highly welcome.

Results and Discussion

This manuscript discusses three kinds of charge schedules: linear, quasi-non-linear, and non-linear. For a linear charge schedule, the derivative by time of the actuated property, e.g., the current, is zero. This is the case for a conventional constant current (CC) - constant voltage (CV) or CCCV protocol, as shown in Figure 1a). A quasi-non-linear charging schedule is when the time derivative of the *actuated* property is non-zero, but that of the *resulting* property is. This is the case for the toy example shown in Figure 1b). There, the *actuated* property is a

non-linear voltage curve (in fact, the same originating from the simulation in Figure 1a) and the *measured* property is the current. As the reader might tell, there are some minor errors in the simulation with the non-linear voltage signal due to imperfect interpolations. The resulting differential capacity plots are shown in Figure 1c) and are virtually indistinguishable. Unsurprising this edge case of non-linear charging produces a conventionally interpretable dQ/dV diagram. Not discussed herein are pulsed protocols, as demonstrated by Garcia et al.[31] and Cicvaric et al., however, these protocols fall into the linear charging category (intermittently stopped). A defining difference is also the fact that these, again, actuate current and not potential.

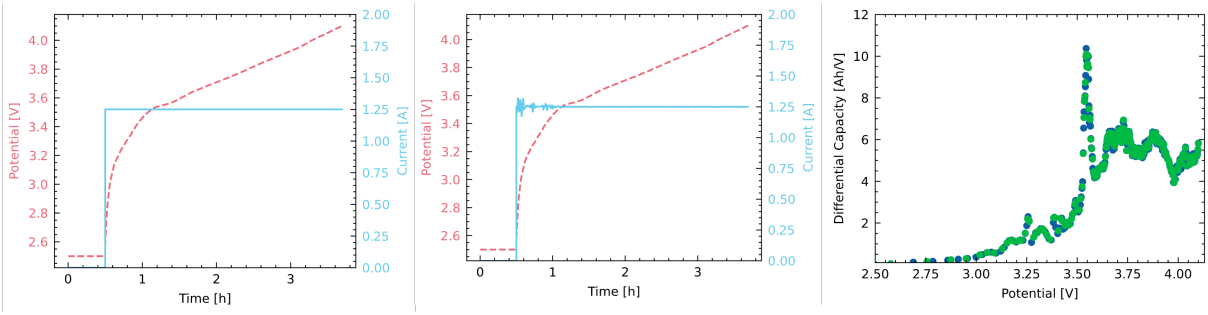

Figure 1: *Current, voltage, and differential capacity plots from charging a simulated cell. On the left in a) a cell is charged using a conventional constant current after a rest of 30 min at a current equivalent of C/4 i.e. a current is applied and a potential is measured. The measured voltage from a) is taken as input for a simulation in b) where the potential is applied and the current is measured. Both simulations yield roughly the same result minding some initial current overshoot due to interpolation errors in b). Both resulting differential capacity plots are also virtually indistinguishable except for having different point densities. This is to demonstrate that even a highly non-linear charging procedure can easily be interpreted. If this charging schedule was to be repeated and certain intercalation reactions were exhibiting changes they would become visible as non-linear current responses. Overall dQ/dV values only deviate by +/- 0.02 Ah within a 80% absolute error band – mostly resulting from interpolation and numerical differentiation errors. The same effect can be obtained for discharging a cell; performing this kind of charge procedure would, however require an arbitrary function generator or the adaption of a drive cycle.*

The next step for quasi-linear battery charging is to perform a conventional linear sweep voltammetry experiment. Here the potential is linearly driven from the OCV to some desired end potential at a constant rate. The resulting dQ/dV plot for this "classic" electrochemical experiment is shown in Figure 2 a)-d) for both a charge and discharge experiment at different sweep rates. Since the time derivate of the potential is constant, the resulting dQ/dV plot also directly entails the shape of the current as dV is constant and essentially dt times a prefactor such that the resulting dQ/dV plot is congruent with the current A(t). The shape is qualitatively similar in that peak positions occur at the same potentials, but the underlying shape is different. A secondary benefit for data analysis is that since the potential is equally spaced the dQ/dV plot is equally spaced along the x-axis as well, making it easier to cross-correlate data as interpolation errors can be mitigated.

To make the standard linear sweep voltammogram a little bit more complex, it can be superimposed with an ultra-low frequency sinusoidal – here on the order of fractions of a mHz with the resulting dQ/dV plot shown in Figure 3. The result is that there are potential areas in the dQ/dV plot that are more whilst others are or less "dense" – however, here by design and not by choice as is the case for CCCV charging. It remains to be tested if the interesting simulatively observed shape, as shown in Figure 3, is really going to be observed in an experiment, but programming battery cyclers with these highly non-linear voltage profiles has proven to be challenging and remains a task for future research in non-linear battery cycling. By increasing the amplitude of the superimposed sinusoidal division by 0 in the dQ/dV (as dV approaches near 0) can be triggered that remains to be

elucidated experimentally as it could trigger dendrite growth or by the very least exciting morphology changes. If the resulting shape of the dQ/dV plot is not observed this could also mark an interesting edge case for some uncaptured physics in the DFN model.

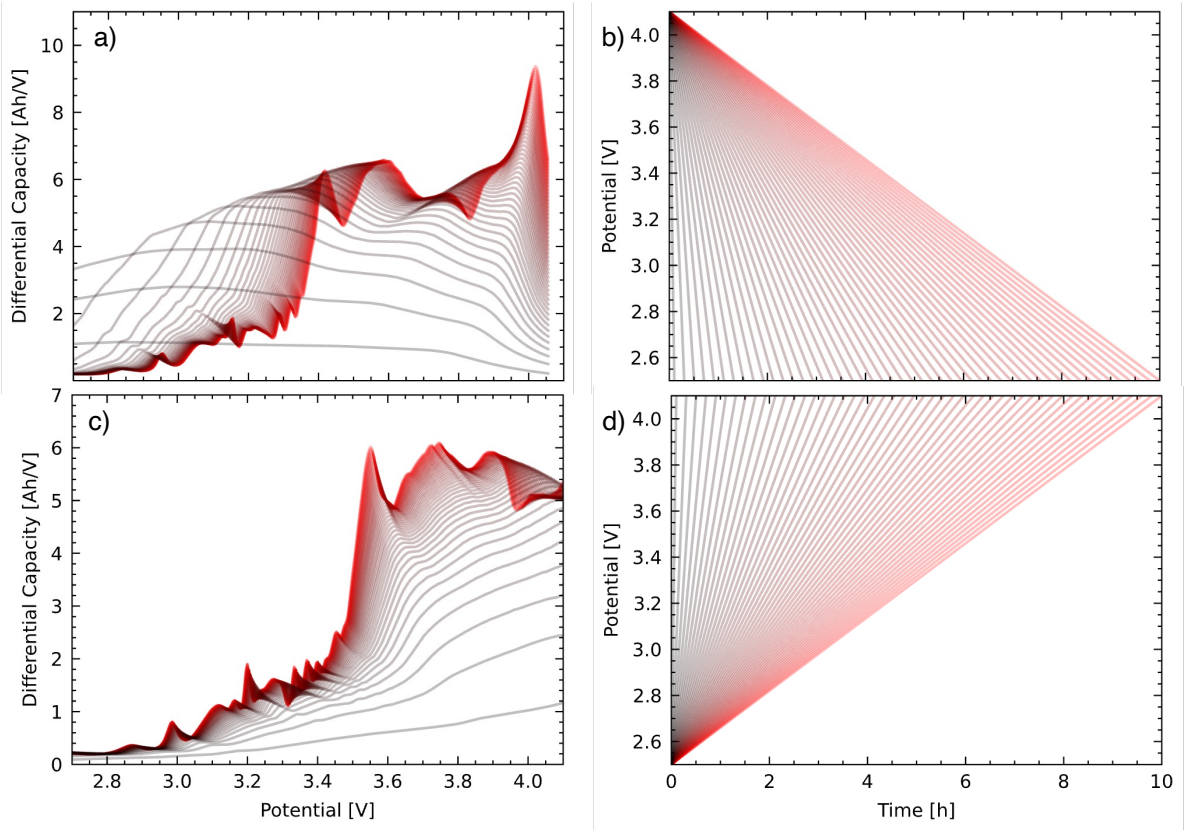

Figure 2: *Differential capacity plots of simulated cells (dis)charged using a linear potential sweep. The resulting dQ/dV plot appears qualitatively different; however, peak positions remain largely the same when charged at an equivalent C/10 rate. The benefit of a linear voltage sweep is that the density of points in the differential capacity plot is constant, and one can omit plotting the current as a function of time as it follows from the shape of the dQ/dV plot as dV=r*dt and dQ/dt=A. If given just the total charging time and rate the dQ/dV plot from a linear sweep voltammetry example is, therefore more information-dense than from a CC experiment.*

Though it may be of interest to increase the area at specific potentials in the dQ/dV diagram but the physical mechanism and interpretation thereof would be interesting to investigate. An even greater interest lies, however in reducing the area under the curve at some potentials. This is due to some intercalation sites or phase transitions associated with increased corrosion, particle cracking, or low reversibility[29,32,33]. Reducing the area under the curve at some potentials can be obtained by superimposing an arctangent (arctan) instead of a sinusoidal onto the linear sweep, as shown in Figure 3. The issue with this method is, however, that if one chooses a fixed total time to charge or effective C-rate (since it is highly variable in this case) the charge needs to be "shoved" into the following higher phase/site at the next higher potential. This leads again to spikes, as observed for the superimposed sinusoidal. One could, of course, try to optimize the ramp slope, potential difference etc. to mitigate this overshoot in differential capacity. If the amplitude of the arctan for the linear sweep voltammetry experiment is lowered to only 0.1V there are still significant overshoots in the dQ/dV plot. A more elegant way is, however to use the quasi-non-linear charging schedule as shown in Figure 1b) and superimpose the previously discussed arctan. The resulting dQ/dV plot is shown in Figure 5. The interesting property here is that the resulting current is non-linear in time (tough essentially linear), not

pulsating as for the superimposed sinusoidal and that there are no dQ/dV overshoots for the herein relatively arbitrarily chosen step height of only 0.1V. This minor alteration has a strong effect of more than nearly halving the differential capacity near the transition potential.

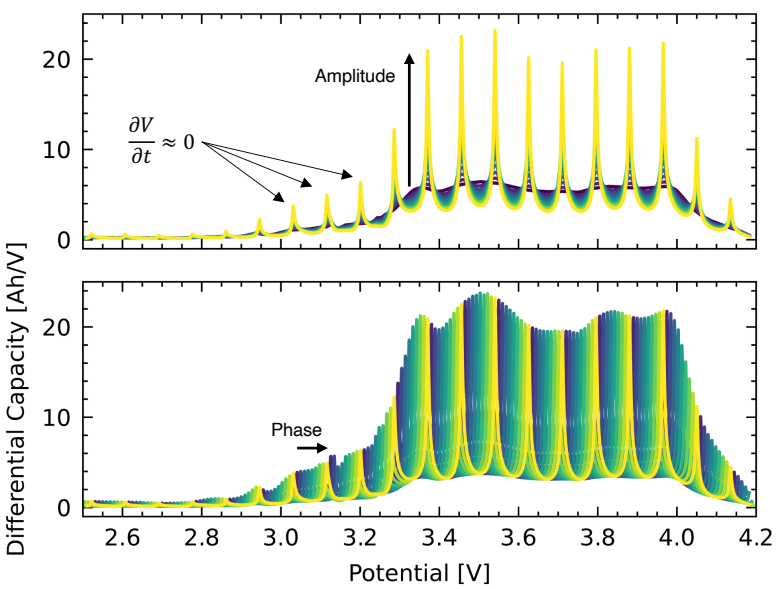

Figure 3: *Differential capacity plots of simulated cells (dis)charged using a linear potential sweep with an overlayed sinusoidal signal. Contrary to figure 2 the time spend at every potential increment i.e. dV/dt is not constant. As there are sections where dV/dt is close to zero one can generate spikes in the differential capacity diagram. Whether or not the extent of these spikes is physical remains to be tested experimentally. The spikes can be exactly placed by adjusting the phase of the superimposed sinusoidal. In between the artificially generated spikes less charge is being intercalated motivating a search for non-linear charging strategies that can omit certain unwanted intercalation sites or phase transitions.*

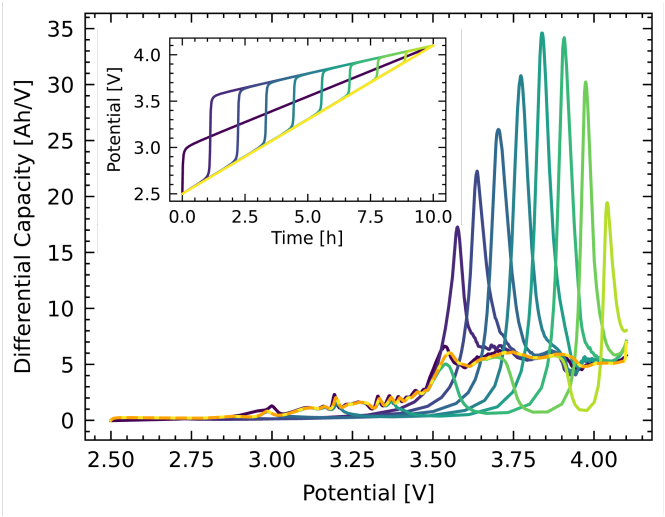

Figure 4: *Differential capacity plot from a linear potential sweep with a superimposed arctan function. Varied are the times at which the arctan was superimposed. The arctan superimposition leads to less time spent at certain potentials i.e. the dime derivate of the potential sweep can be decreased. This leads to the omission of some potentials in the dQ/dV plot. Since this is a full cell simulation the omitted potential ranges can relate to the chemical potentials of phases in the anode and cathode.*

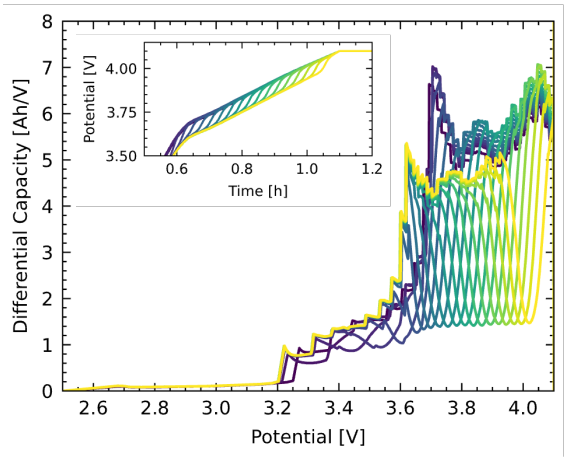

Figure 5: *Differential capacity plots for a non-linear charge schedule that is derived from the same idea as in Figure 1 i.e. applying a non-linear voltage to obtain a perfectly constant current, however, superimposed onto that voltage signal is an arctan function at different times. This leads to a partially non-linear response in the current but most importantly a selective diminishing of the differential capacity at some potentials. The inset shows a section of the applied voltage. Contrary to the other simulations this model models EC reaction limited SEI growth with distributed film resistance, porosity changes and irreversible Li-plating with porosity change.*

Interestingly there are no overshoots either, as the slope of the voltage after the arctan step corresponds to the (non-linear) voltage signal necessary to yield a similar C-rate. As a toy example, one can now look at the Li-loss to the SEI for different positions of the superimposed arctan in time as shown in Figure 6, after a CV step to C/50. This CC step is to ensure that despite the different charge schedules all data shown corresponds to the same SOC (though not charge time). The data suggests that Li-Loss to the SEI can be reduced if the arctan onto the non-linear voltage signal is superimposed at the right potential (roughly 3.75-3.8V). This potential is the chosen example associated with a phase transition/reduction in the NMC811[32]. With this plot at different C-rates one could start to construct a diagram showing potential ranges to be avoided during charging and, if shifting in potential by C-rate, help to construct a map of C-rate dependent "instability" ranges.

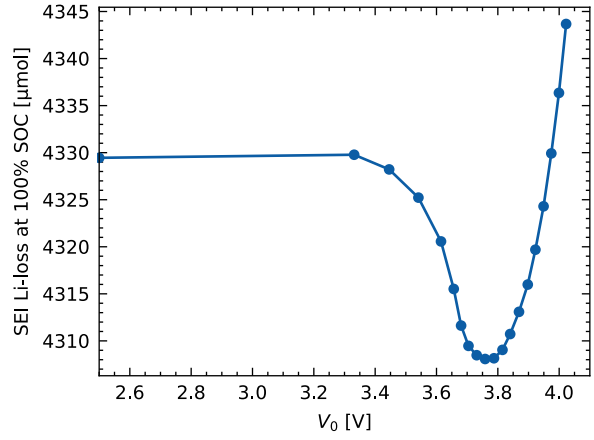

Figure 6: *Li-loss to the SEI after the non-linear charging procedure with a superimposed arctan. The x-axis shows the inflection point V_0 of the arctan and the Li-loss is reported after holding the simulated cell at the maximum voltage until a C/50 equivalent current is reached (herein reported as 100% SOC). This plot suggests that reducing the integral capacity in the voltage range of 3.7-3.8V leads to less Li-loss to the SEI. These numbers are to be viewed with caution as they are highly dependent on the implementation, discretization etc., and should solely demonstrate a general trend.*

Conclusion

This manuscript explored linear, quasi-non-linear, and on linear charging of batteries. The motivation is first and foremost an interesting toy example where a battery is potentiodynamically charged in such a way that the current

remains constant - yielding virtually the same dQ/dV plots. This example is further explored using classic linear sweep voltammetry to yield information-dense dQ/dV plots that contain the congruent shape of the non-linear current response. Superimposing a sinusoidal onto a linear sweep voltammogram of a battery is then shown to be able to yield spikes in the differential capacity plot whose physical manifestation in an experiment remains to be validated. Superimposing an arctan onto a linear sweep voltammogram enables to reduce the area at selected potentials in the dQ/dV plot but yields overshoots in the dQ/dV diagram at higher potentials. Superimposing an arctan onto a non-linear potentiodynamic schedule that would have produced a constant current response mitigates these overshoots and enables the selective omission of potential ranges in the differential capacity plot. After fully charging the simulated cell there is a minimum in Li-loss to the SEI that can be correlated with phase transitions occurring in the cathode, in the chosen example NMC811, that are mitigated. The presented study is an entirely simulative endeavor and remains to be experimentally validated in future research.

Engineering highly non-linear charging schedules has implications in formation and cell aging. If it is possible to selectively omit (or emphasize) the intercalation or phase transition at select potentials, this markes a new "engineering lever" to pull, allowing to alter the growth of the SEI only electrochemically and not diffusive as for instance done in Cicvaric et al.[34] and Garcia et al.[31] for metal electrodes. Expressed differently: Applying a non-trivial non-linear voltage or current signal onto a battery creates the opportunity to **intentionally** activate or mitigate some corrosion mechanisms. Since the resulting graphs as Figure 6 allow the correlation to mechanisms in the anode/cathode at different c-rates it becomes possible to construct Pourbaix-like diagrams of potential ranges to avoid. This diagram could then directly contribute to the engineering of both electrochemical processes and engineering of the SEI composition during formation and use.

Acknowledgements

This research received funding from the Deutsche Forschungsgemeinschaft (DFG, German Research Foundation) under Germany´s Excellence Strategy – EXC 2089/1 – 390776260.**References**

(1) Amici, J.; Asinari, P.; Ayerbe, E.; Barboux, P.; Bayle-Guillemaud, P.; Behm, R. J.; Berecibar, M.; Berg, E.; Bhowmik, A.; Bodoardo, S.; Castelli, I. E.; Cekic-Laskovic, I.; Christensen, R.; Clark, S.; Diehm, R.; Dominko, R.; Fichtner, M.; Franco, A. A.; Grimaud, A.; Guillet, N.; Hahlin, M.; Hartmann, S.; Heiries, V.; Hermansson, K.; Heuer, A.; Jana, S.; Jabbour, L.; Kallo, J.; Latz, A.; Lorrmann, H.; Løvvik, O. M.; Lyonnard, S.; Meeus, M.; Paillard, E.; Perraud, S.; Placke, T.; Punckt, C.; Raccurt, O.; Ruhland, J.; Sheridan, E.; Stein, H.; Tarascon, J.-M.; Trapp, V.; Vegge, T.; Weil, M.; Wenzel, W.; Winter, M.; Wolf, A.; Edström, K. A Roadmap for Transforming Research to Invent the Batteries of the Future Designed within the European Large Scale Research Initiative BATTERY 2030+. *Adv. Energy Mater.* **2022**, *12* (17), 1–42. https://doi.org/10.1002/aenm.202102785.

(2) Bhowmik, A.; Berecibar, M.; Casas-Cabanas, M.; Csanyi, G.; Dominko, R.; Hermansson, K.; Palacin, M. R.; Stein, H. S.; Vegge, T. Implications of the BATTERY 2030+ AI-Assisted Toolkit on Future Low-TRL Battery Discoveries and Chemistries. *Adv. Energy Mater.* **2021**, 2102698.

(3) Bhowmik, A.; Castelli, I. E.; Garcia-Lastra, J. M.; Jørgensen, P. B.; Winther, O.; Vegge, T. A Perspective on Inverse Design of Battery Interphases Using Multi-Scale Modelling, Experiments and Generative

Deep Learning. *Energy Storage Mater.* **2019**, *21*, 446–456. https://doi.org/10.1016/j.ensm.2019.06.011.
(4) Friederich, P.; Häse, F.; Proppe, J.; Aspuru-Guzik, A. Machine-Learned Potentials for next-Generation Matter Simulations. *Nat. Mater.* **2021**, *20* (6), 750–761. https://doi.org/10.1038/s41563-020-0777-6.
(5) Choudhary, N.; Clever, H.; Ludwigs, R.; Rath, M.; Gannouni, A.; Schmetz, A.; Hülsmann, T.; Sawodny, J.; Fischer, L.; Kampker, A.; Fleischer, J.; Stein, H. S. Autonomous Visual Detection of Defects from Battery Electrode Manufacturing. *Adv. Intell. Syst.* **2022**, *4* (12), 2200142. https://doi.org/10.1002/aisy.202200142.
(6) Vogler, M.; Busk, J.; Hajiyani, H.; Jørgensen, P. B.; Safaei, N.; Castelli, I.; Ramírez, F. F.; Carlsson, J.; Pizzi, G.; Clark, S.; Hanke, F.; Bhowmik, A.; Stein, H. S. *Brokering between Tenants for an International Materials Acceleration Platform*; preprint; Chemistry, 2022. https://doi.org/10.26434/chemrxiv-2022-grgrd.
(7) Stein, H. S.; Sanin, A.; Rahmanian, F.; Zhang, B.; Vogler, M.; Flowers, J. K.; Fischer, L.; Fuchs, S.; Choudhary, N.; Schroeder, L. From Materials Discovery to System Optimization by Integrating Combinatorial Electrochemistry and Data Science. *Curr. Opin. Electrochem.* **2022**, 101053.
(8) Rahmanian, F.; Vogler, M.; Wölke, C.; Yan, P.; Winter, M.; Cekic-Laskovic, I.; Stein, H. S. One-Shot Active Learning for Globally Optimal Battery Electrolyte Conductivity**. *Batter. Supercaps* **2022**, *5* (10). https://doi.org/10.1002/batt.202200228.
(9) Häse, F.; Roch, L. M.; Aspuru-Guzik, A. Chimera: Enabling Hierarchy Based Multi-Objective Optimization for Self-Driving Laboratories. *Chem. Sci.* **2018**, *9* (39), 7642–7655. https://doi.org/10.1039/C8SC02239A.
(10) Häse, F.; Roch, L. M.; Kreisbeck, C.; Aspuru-Guzik, A. Phoenics: A Bayesian Optimizer for Chemistry. *ACS Cent. Sci.* **2018**, *4* (9), 1134–1145. https://doi.org/10.1021/acscentsci.8b00307.
(11) Häse, F.; Roch, L. M.; Aspuru-Guzik, A. Next-Generation Experimentation with Self-Driving Laboratories. *Trends Chem.* **2019**, *1* (3), 282–291. https://doi.org/10.1016/j.trechm.2019.02.007.
(12) Burns, J. C.; Petibon, R.; Nelson, N.; Sinha, N. N.; Kassam, A.; Way, B. M.; Dahn, J. R. Studies of the Effect of Varying Vinylene Carbonate (VC) Content in Lithium Ion Cells on Cycling Performance and Cell Impedance. *J. Electrochem. Soc.* **2013**, *160*. https://doi.org/10.1149/2.031310jes.
(13) Blaiszik, B.; Ward, L.; Schwarting, M.; Gaff, J.; Chard, R.; Pike, D.; Chard, K.; Foster, I. A Data Ecosystem to Support Machine Learning in Materials Science. *MRS Commun.* **2019**, *9* (4), 1125–1133. https://doi.org/10.1557/mrc.2019.118.
(14) Balachandran, P. V. Machine Learning Guided Design of Functional Materials with Targeted Properties. *Comput. Mater. Sci.* **2019**, *164*, 82–90. https://doi.org/10.1016/j.commatsci.2019.03.057.
(15) Correa-Baena, J.-P.; Hippalgaonkar, K.; van Duren, J.; Jaffer, S.; Chandrasekhar, V. R.; Stevanovic, V.; Wadia, C.; Guha, S.; Buonassisi, T. Accelerating Materials Development via Automation, Machine Learning, and High-Performance Computing. *Joule* **2018**, *2* (8), 1410–1420. https://doi.org/10.1016/j.joule.2018.05.009.
(16) Ho Gu, G.; Noh, J.; Kim, I.; Jung, Y. Machine Learning for Renewable Energy Materials. *J. Mater. Chem. A* **2019**. https://doi.org/10.1039/C9TA02356A.
(17) Stein, H. S.; Guevarra, D.; Newhouse, P. F.; Soedarmadji, E.; Gregoire, J. M. Machine Learning of Optical Properties of Materials – Predicting Spectra from Images and Images from Spectra. *Chem. Sci.* **2019**, *10* (1), 47–55. https://doi.org/10.1039/C8SC03077D.
(18) Stein, H. S. Advancing Data-Driven Chemistry by Beating Benchmarks. *Trends Chem.* **2022**.
(19) Rohr, B.; Stein, H. S.; Guevarra, D.; Wang, Y.; Haber, J. A.; Aykol, M.; Suram, S. K.; Gregoire, J. M. Benchmarking the Acceleration of Materials Discovery by Sequential Learning. *Chem. Sci.* **2020**, *11* (10), 2696–2706. https://doi.org/10.1039/C9SC05999G.
(20) Attia, P. M.; Grover, A.; Jin, N.; Severson, K. A.; Markov, T. M.; Liao, Y.-H.; Chen, M. H.; Cheong, B.; Perkins, N.; Yang, Z.; Herring, P. K.; Aykol, M.; Harris, S. J.; Braatz, R. D.; Ermon, S.; Chueh, W. C. Closed-Loop Optimization of Fast-Charging Protocols for Batteries with Machine Learning. *Nature* **2020**, *578* (7795), 397–402. https://doi.org/10.1038/s41586-020-1994-5.
(21) Herring, P.; Balaji Gopal, C.; Aykol, M.; Montoya, J. H.; Anapolsky, A.; Attia, P. M.; Gent, W.; Hummelshøj, J. S.; Hung, L.; Kwon, H.-K.; Moore, P.; Schweigert, D.; Severson, K. A.; Suram, S.; Yang, Z.; Braatz, R. D.; Storey, B. D. BEEP: A Python Library for Battery Evaluation and Early Prediction. *SoftwareX* **2020**, *11*, 100506. https://doi.org/10.1016/j.softx.2020.100506.
(22) Rieger, L. H.; Flores, E.; Nielsen, K. F.; Norby, P.; Ayerbe, E.; Winther, O.; Vegge, T.; Bhowmik, A. Uncertainty-Aware and Explainable Machine Learning for Early Prediction of Battery Degradation Trajectory. *Digit. Discov.* **2023**, *2* (1), 112–122. https://doi.org/10.1039/D2DD00067A.
(23) Stein, H. S.; Gregoire, J. M. Progress and Prospects for Accelerating Materials Science with Automated and Autonomous Workflows. *Chem. Sci.* **2019**, No. 10.1039/C9SC03766G.
(24) Flores, E.; Wölke, C.; Yan, P.; Winter, M.; Vegge, T.; Cekic-Laskovic, I.; Bhowmik, A. Learning the Laws of Lithium-Ion Transport in Electrolytes Using Symbolic Regression. *Digit. Discov.* **2022**, *1* (4), 440–447. https://doi.org/10.1039/D2DD00027J.
(25) Flores, E.; Åvall, G.; Jeschke, S.; Johansson, P. Solvation Structure in Dilute to Highly Concentrated Electrolytes for Lithium-Ion and Sodium-Ion Batteries. *Electrochimica Acta* **2017**, *233*, 134–141. https://doi.org/10.1016/j.electacta.2017.03.031.

(26) Zhang, B.; Merker, L.; Sanin, A.; Stein, H. S. Robotic Cell Assembly to Accelerate Battery Research. *Digit. Discov.* **2022**, *1* (6), 755–762. https://doi.org/10.1039/D2DD00046F.
(27) Smith, A. J.; Burns, J. C.; Dahn, J. R. High-Precision Differential Capacity Analysis of $LiMn_2O_4$/Graphite Cells. *Electrochem. Solid-State Lett.* **2011**, *14* (4), A39–A41. https://doi.org/10.1149/1.3543569.
(28) Badiali, J. P.; Rosinberg, M. L.; Goodisman, J. Contribution of the Metal to the Differential Capacity of an Ideally Polarisable Electrode. *J. Electroanal. Chem. Interfacial Electrochem.* **1983**, *143* (1–2), 73–88. https://doi.org/10.1016/S0022-0728(83)80255-1.
(29) Sulzer, V.; Marquis, S. G.; Timms, R.; Robinson, M.; Chapman, S. J. Python Battery Mathematical Modelling (PyBaMM). *J. Open Res. Softw.* **2021**, *9* (1), 14. https://doi.org/10.5334/jors.309.
(30) O'Kane, S. E. J.; Ai, W.; Madabattula, G.; Alonso-Alvarez, D.; Timms, R.; Sulzer, V.; Edge, J. S.; Wu, B.; Offer, G. J.; Marinescu, M. Lithium-Ion Battery Degradation: How to Model It. *Phys. Chem. Chem. Phys.* **2022**, *24* (13), 7909–7922. https://doi.org/10.1039/D2CP00417H.
(31) Garcia, G.; Ventosa, E.; Schuhmann, W. Complete Prevention of Dendrite Formation in Zn Metal Anodes by Means of Pulsed Charging Protocols. *ACS Appl. Mater. Interfaces* **2017**, *9* (22), 18691–18698. https://doi.org/10.1021/acsami.7b01705.
(32) Jung, R.; Metzger, M.; Maglia, F.; Stinner, C.; Gasteiger, H. A. Oxygen Release and Its Effect on the Cycling Stability of $LiNi_xMn_yCo_zO_2$ (NMC) Cathode Materials for Li-Ion Batteries. *J. Electrochem. Soc.* **2017**, *164* (7), A1361–A1377. https://doi.org/10.1149/2.0021707jes.
(33) Sauer, D. U. Time-Series Cyclic Aging Data on 48 Commercial NMC/Graphite Sanyo/Panasonic UR18650E Cylindrical Cells, 2021. https://doi.org/10.18154/RWTH-2021-04545.
(34) Cicvarić, K.; Merker, L.; Zhang, B.; Gaberšček, M.; Stein, H. S. *Fast Formation of Anode-Free Li-Metal Batteries by Pulsed Current*; preprint; Chemistry, 2023. https://doi.org/10.26434/chemrxiv-2023-s49kw.